7

Tangential loading and sliding contact

7.1 Sliding of non-conforming elastic bodies

In our preliminary discussion in Chapter 1 of the relative motion and forces which can arise at the point of contact of non-conforming bodies we distinguished between the motion described as *sliding* and that described as *rolling*. Sliding consists of a relative peripheral velocity of the surfaces at their point of contact, whilst rolling involves a relative angular velocity of the two bodies about axes parallel to their tangent plane. Clearly rolling and sliding can take place simultaneously, but in this chapter we shall exclude rolling and restrict our discussion to the contact stresses in simple rectilinear sliding. The system is shown in Fig. 7.1. A slider, having a curved profile, moves from right to left over a flat surface. Following the approach given in Chapter 1, we regard the point of initial contact as a fixed origin and imagine the material of the lower surface flowing through the contact region from left to right with a steady velocity V. For convenience we choose the x-axis parallel to the direction of sliding.

Fig. 7.1. Sliding contact.

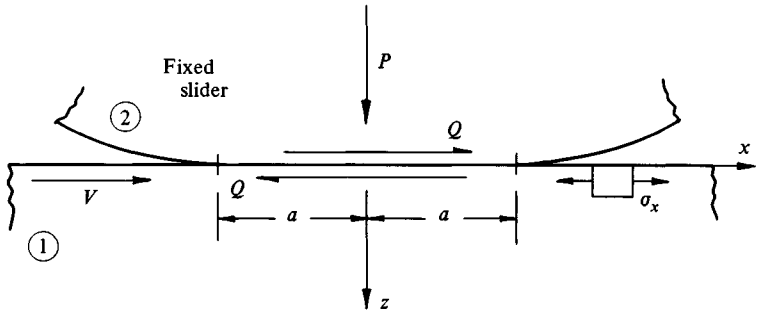

https://doi.org/10.1017/CBO9781139171731.008 Published online by Cambridge University Press

A normal force P pressing the bodies together gives rise to an area of contact which, in the absence of friction forces, would have dimensions given by the Hertz theory. Thus in a frictionless contact the contact stresses would be unaffected by the sliding motion. However a sliding motion, or any tendency to slide, of real surfaces introduces a tangential force of friction Q, acting on each surface, in a direction which opposes the motion. We are concerned here with the influence of the tangential force Q upon the contact stresses. In this section we shall imagine that the bodies have a steady sliding motion so that the force Q represents the force of 'kinetic friction' between the surfaces. In the next section we shall investigate the situation of two bodies, nominally with no relative velocity, but subjected to a tangential force tending to cause them to slide. The force Q then arises from 'static friction'; it may take any value which does not exceed the force of 'limiting friction' when sliding is just about to occur.

The first question to consider is whether the tangential traction due to friction at the contact surface influences the size and shape of the contact area or the distribution of normal pressure. For the purposes of calculating the elastic stresses and displacements due to the tangential tractions, we retain the basic premise of the Hertz theory that the two bodies can each be regarded as an elastic half-space in the proximity of the contact region. The methods of analysis given in Chapter 2 and 3 are then appropriate. From equation (2.22) in two dimensions and from equation (3.75) in three dimensions we note that the *normal* component of displacement at the surface $\bar{u}_z$ due to a concentrated *tangential* force Q is proportional to the elastic constant $(1-2\nu)/G$. The tangential tractions acting on each surface at the interface are equal in magnitude and opposite in direction, viz.:

$$q_1(x,y) = -q_2(x,y) \tag{7.1}$$

Hence the normal displacements due to these tractions are proportional to the respective values of $(1-2\nu)/G$ of each body and are of opposite sign:

$$\frac{G_1}{1-2\nu_1}\bar{u}_{z1}(x,y) = -\frac{G_2}{1-2\nu_2}\bar{u}_{z2}(x,y) \tag{7.2}$$

It follows from equation (7.2) that, if the two solids have the same elastic constants, any tangential traction transmitted between them gives rise to equal and opposite normal displacements of any point on the interface. Thus the warping of one surface conforms exactly with that of the other and does not disturb the distribution of normal pressure. The shape and size of the contact area are then fixed by the profiles of the two surfaces and the normal force, and are independent of the tangential force. With solids of different elastic properties this is no longer the case and the tangential tractions do interact with

the normal pressure. The effect is entirely analogous to the interaction between normal and tangential tractions in normal contact of dissimilar solids discussed in §5.4. However, as we shall see later, it transpires that the influence of tangential tractions upon the normal pressure and the contact area is generally small, particularly when the coefficient of limiting friction is appreciably less than unity. In our analysis of problems involving tangential tractions, therefore, we shall neglect this interaction and assume that the stresses and deformation due to (*a*) the normal pressure and (*b*) the tangential traction are independent of each other, and that they can be superposed to find the resultant stress.

We must now prescribe the relationship between the tangential traction and the normal pressure in sliding contact. It is usual to assume that Amontons' law of sliding friction applies at each elementary area of the interface, so that

$$\frac{|q(x,y)|}{p(x,y)} = \frac{|Q|}{P} = \mu \tag{7.3}$$

where μ is a constant coefficient of kinetic friction whose value is determined by the materials and the physical conditions of the interface. Some indication of the circumstances which account for the validity of Amonton's law with dry surfaces can be found in Chapter 13. It is also found to be approximately valid when *non-conforming* sliding surfaces are separated by thin lubricating films. Experimental confirmation that the tangential traction is distributed in direct proportion to normal pressure is provided by photo-elastic work of Ollerton & Haines (1963) using large models of araldite epoxy resin. For a full discussion of the physics of friction and the conditions which determine the value of the coefficient of friction, the reader is referred to Bowden & Tabor (1951, 1964).

We are now in a position to examine the elastic stress distributions in sliding contact. The two-dimensional case of a cylinder sliding in a direction perpendicular to its axis has been studied in more detail than the corresponding three-dimensional case. We will look at the two-dimensional problem first:

(a) Cylinder sliding perpendicular to its axis

If the cylinder and the plane on which it slides have the same elastic properties, we have seen that the width of the contact strip $2a$ and the normal pressure distribution are given by the Hertz theory (equations (4.43)–(4.45)), i.e.

$$p(x) = \frac{2P}{\pi a^2}(a^2 - x^2)^{1/2}$$

where P is the normal force per unit axial length pressing the cylinder into contact with the plane. Then, assuming Amonton's law of friction (equation

(7.3)) the tangential traction is

$$q(x) = \mp \frac{2\mu P}{\pi a^2} (a^2 - x^2)^{1/2} \tag{7.4}$$

where the negative sign is associated with a positive velocity V as shown in Fig. 7.1. The stress components within both the cylinder and the plane are now given by equations (2.23). These integrals have been evaluated by several workers (McEwen, 1949; Poritsky, 1950; Smith & Liu, 1953; Sackfield & Hills, 1983*c*). A short table of values is given in Appendix 4. From equations (2.23), since $q(x)$ and $p(x)$ are in proportion, it may be seen that there are some analogies between the stresses due to the tangential traction and those due to the normal traction, which may be expressed by:

$$\frac{(\sigma_z)_q}{q_0} = \frac{(\tau_{xz})_p}{p_0} \tag{7.5a}$$

and

$$\frac{(\tau_{xz})_q}{q_0} = \frac{(\sigma_x)_p}{p_0} \tag{7.5b}$$

where $q_0 = \mu p_0$ is the tangential traction at $x = 0$, and the suffixes p and q refer to stress components due to the normal pressure and tangential traction acting separately. Hence $(\sigma_z)_q$ and $(\tau_{xz})_q$ can be found directly from the expressions for $(\tau_{xz})_p$ and $(\sigma_x)_p$ given by equations (4.49). The direct stress parallel to the surface $(\sigma_x)_q$, however, must be evaluated independently. In the notation of equations (4.49) it may be shown that

$$(\sigma_x)_q = \frac{q_0}{a}\left\{n\left(2 - \frac{z^2 - m^2}{m^2 + n^2}\right) - 2x\right\}^{\dagger} \tag{7.6}$$

At the surface $z = 0$ the expression for the direct stress reduces to:

$$(\bar{\sigma}_x)_q = \begin{cases} -2q_0 x/a, & |x| \leqslant a \qquad (7.7a) \\ -2q_0\left\{\dfrac{x}{a} \mp \left(\dfrac{x^2}{a^2} - 1\right)^{1/2}\right\}, & |x| > a \qquad (7.7b) \end{cases}$$

The surface stresses in the moving plane (Fig. 7.1) are shown in Fig. 7.2. The tangential traction acting on the moving plane is negative so that the direct stress reaches a maximum compressive stress $-2q_0$ at the leading edge of the contact area ($x = -a$) and a maximum tension $2q_0$ at the trailing edge ($x = a$). We recall that the normal pressure gives rise to an equal compressive stress at the surface, $(\sigma_x)_p = -p(x)$, within the contact region and no stress outside. Hence, whatever the coefficient of friction, the maximum resultant tensile stress in sliding contact occurs at the trailing edge with the value $2\mu p_0$.

† A short table of values is given in Appendix 4 (p. 430).

https://doi.org/10.1017/CBO9781139171731.008 Published online by Cambridge University Press

The onset of plastic yield in sliding contact will be governed (using the Tresca yield criterion) by the maximum value of the principal shear stress throughout the field. Contours of τ_1 in the absence of friction are shown in Fig. 4.5. The maximum value is $0.30p_0$ on the z-axis at a depth $0.78a$. Contours of τ_1 due to combined normal pressure and tangential traction, taking $\mu = 0.2$, are plotted in Fig. 7.3. The maximum value now occurs at a point closer to the surface. The position and magnitude of the maximum principal shear stress may be computed and equated to the yield stress k in simple shear to find the contact pressure p_0 for first yield (by the Tresca yield criterion). This is shown for increasing values of the coefficient of friction in Fig. 7.4. The frictional traction also introduces shear stresses into the contact surface which can reach yield if the coefficient of friction is sufficiently high. The stresses in the contact surface

Fig. 7.2. Surface stresses due to frictional traction $q = q_0(1 - x^2/a^2)^{1/2}$.

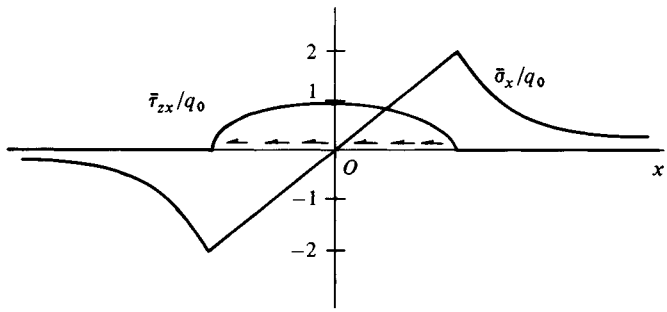

Fig. 7.3. Contours of the principal shear stress τ_1 beneath a sliding contact, $Q_x = 0.2P$.

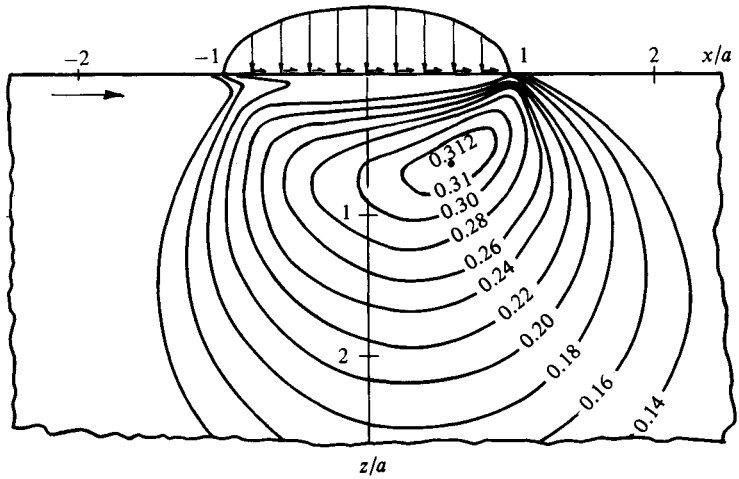

https://doi.org/10.1017/CBO9781139171731.008 Published online by Cambridge University Press

due to both pressure and frictional tractions are

$$\bar{\sigma}_x = -p_0\{(1-x^2/a^2)^{1/2} + 2\mu x/a\} \tag{7.8a}$$

$$\bar{\sigma}_z = -p_0(1-x^2/a^2)^{1/2} \tag{7.8b}$$

$$\bar{\sigma}_y = -2\nu p_0\{(1-x^2/a^2)^{1/2} + \mu x/a\} \tag{7.8c}$$

$$\bar{\tau}_{xz} = -\mu p_0(1-x^2/a^2)^{1/2} \tag{7.8d}$$

The principal shear stress in the plane of the deformation is

$$\tau_1 = \tfrac{1}{2}\{(\sigma_x - \sigma_z)^2 + 4\tau_{xz}^2\}^{1/2} = \mu p_0 \tag{7.9}$$

This result shows that the material throughout the width of the contact surface will reach yield when

$$p_0/k = 1/\mu \tag{7.10}$$

Yield may also occur by 'spread' of the material in the axial direction although such flow must of necessity be small by the restriction of plane strain. Calculations of the contact pressure for the onset of yield in sliding contact have been made by Johnson & Jefferis (1963) using both the Tresca and von Mises yield criteria; the results are shown in Fig. 7.4. For low values of the coefficient of friction ($\mu < 0.25$ by Tresca and $\mu < 0.30$ by von Mises) the yield point is first reached at a point in the material beneath the contact surface. For larger values of μ yield first occurs at the contact surface. The Tresca criterion predicts lateral yield for $0.25 < \mu < 0.44$; but when $\mu > 0.44$ the onset of yield is given by equation (7.9).

In the above discussion the tangential traction has been assumed to have no effect upon the normal pressure. This is strictly true only when the elastic constants of the two bodies are the same. The influence of a difference in elastic constants has been analysed by Bufler (1959) using the methods of §2.7. The boundary condition $q(x) = \mu p(x)$ is of class IV, which leads to a singular integral equation of the second kind (2.53). Solving the integral equation by (2.55) and (2.56), the surface traction within the contact area is found to be:

$$q(x) = \frac{\mu E^*}{2R(1+\beta^2\mu^2)^{1/2}}\left(\frac{a+x}{a-x}\right)^{\gamma}(a^2-x^2)^{1/2} \tag{7.11}$$

where β is a measure of the difference in the elastic constants defined in equation (5.3) and

$$\gamma = -(1/\pi)\tan^{-1}(\beta\mu) \approx -\beta\mu/\pi \tag{7.12}$$

provided that $\beta\mu$ is small. The semi-width of the contact strip is given by

$$a^2 = \frac{1}{1-4\gamma^2}\frac{4PR}{E^*} \tag{7.13}$$

The contact strip is no longer symmetrically placed; its centre is displaced from

https://doi.org/10.1017/CBO9781139171731.008 Published online by Cambridge University Press

the axis of symmetry by a distance

$$x_0 = 2\gamma a \tag{7.14}$$

Bufler also finds the distribution of direct stress σ_x in the surface. When the elastic constants of the two bodies are equal, β is zero and hence γ vanishes. The contact area is then seen to be symmetrical and of a size given by the Hertz theory; the pressure distribution also reduces to that of Hertz. Values of β for various combinations of materials are given in Table 5.1. The values do not exceed 0.21. Since coefficients of friction rarely exceed 1.0, the maximum likely value of $|\gamma|$ is about 0.06. The distribution of surface traction and contact area have been calculated from equations (7.11)-(7.13), taking $\gamma = 0.06$, for the arrangement in Fig. 7.1 in which it has been assumed that the lower surface

Fig. 7.4. Effect of sliding friction on the contact pressure for first yield and shakedown (see §9.2). Large-dashed line – line contact, first yield (Tresca). Chain line – line contact, first yield (von Mises). Solid line – line contact, shakedown (Tresca). Small-dashed line – point contact, first yield (von Mises).

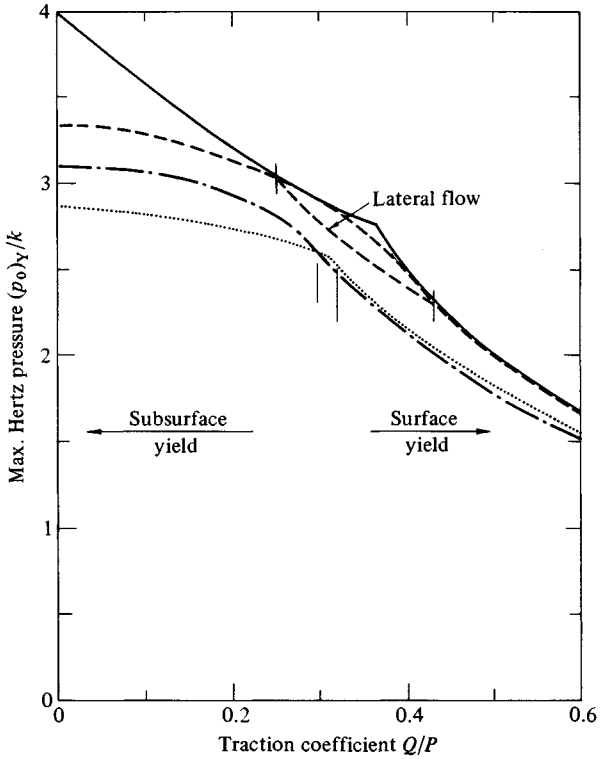

https://doi.org/10.1017/CBO9781139171731.008 Published online by Cambridge University Press

is the more elastic (i.e. β + ve and μ − ve). The results are shown in Fig. 7.5. The effect of the tangential traction is to shift the centre of the contact region by a distance $x_0 = 0.12a$ towards the trailing edge; the contact width is increased by 0.8% and the centre of pressure moves towards the trailing edge. However the comparison with the Hertz pressure distribution shows that the effect is small even for an extreme value of the product $\beta\mu$. For more representative values of $\beta\mu$ the influence of frictional traction upon the contact area and pressure distribution is negligible.

(b) Sliding sphere

We now consider a sphere, carrying a normal load P, which slides over a plane surface in a direction chosen parallel to the x-axis. Neglecting any interaction between normal pressure and tangential traction arising from a difference in elastic constants of the two solids, the size of the circular contact area and the pressure distribution are given by the Hertz theory (equations (3.39), (4.22) and (4.24)). Amontons' law of friction specifies the tangential traction to be

$$q(r) = \frac{3\mu P}{2\pi a^3}(a^2 - r^2)^{1/2} \tag{7.15}$$

acting parallel to the x-axis everywhere in the contact area.

We wish to find the stress components in the solid produced by the surface traction. In principle they may be found by using the stress components due to a concentrated force, given by equations (3.76), weighted by the distribution

Fig. 7.5. Influence of a difference in elastic constants on the pressure and traction distribution in sliding contact, for $\beta = 0.2, \mu = 1$ ($\gamma = 0.06$).

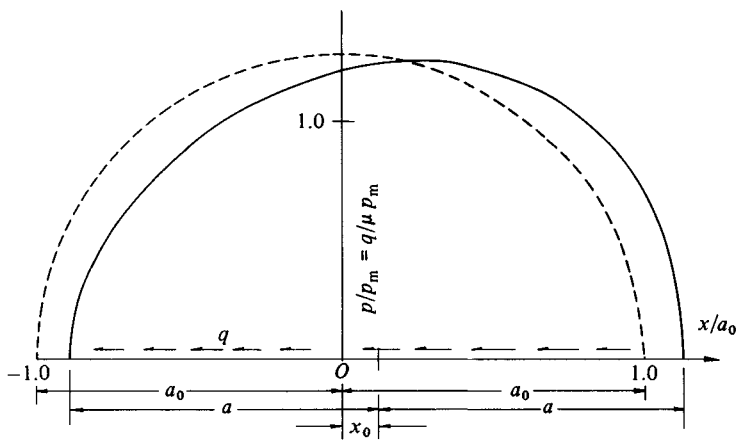

https://doi.org/10.1017/CBO9781139171731.008 Published online by Cambridge University Press

(7.15) and integrated throughout the contact area. However such integrations can only be performed numerically. A different approach has been taken by Hamilton & Goodman (1966), by extending a method introduced by Green (1949) for the stress analysis of a normally loaded half-space. They computed stresses in the x–z plane and at the surface (x–y plane) for values of $\mu = 0.25$ and 0.50, ($\nu = 0.3$). Explicit equations for calculating the stress components at any point in the solid have since been given by Hamilton (1983) and by Sackfield & Hills (1983*c*).

The von Mises criterion has been used to calculate the point of first yield. As for a two-dimensional contact, the point of first yield moves towards the surface as the coefficient of friction is increased; yield occurs at the surface when μ exceeds 0.3. The values of the maximum contact pressure $(p_0)_Y$ to initiate yield have been added to Fig. 7.4 from which it will be seen that they are not significantly different from the two-dimensional case.

The normal contact of elastic spheres introduces a radial tension at $r = a$ of magnitude $(1-2\nu)p_0/3 \approx 0.13p_0$. The effect of the tangential traction is to add to the tension on one side of the contact and to subtract from it at the other. The maximum tension, which occurs at the surface point $(-a, 0)$ rises to $0.5p_0$ and $1.0p_0$ for $\mu = 0.25$ and 0.5 respectively. This result is again comparable with the two-dimensional case.

The analysis has been extended to elliptical contacts by Bryant & Keer (1982) and by Sackfield & Hills (1983*b*) who show that the contact pressure for first yield $(p_0)_Y$ is almost independent of the shape of the contact ellipse.

7.2 Incipient sliding of elastic bodies

A tangential force whose magnitude is less than the force of limiting friction, when applied to two bodies pressed into contact, will not give rise to a sliding motion but, nevertheless, will induce frictional tractions at the contact interface. In this section we shall examine the tangential surface tractions which arise from a combination of normal and tangential forces which does not cause the bodies to slide relative to each other.

The problem is illustrated in Fig. 7.6. The normal force P gives rise to a contact area and pressure distribution which we assume to be uninfluenced by the existence of the tangential force Q, and hence to be given by the Hertz theory. The effect of the tangential force Q is to cause the bodies to deform in shear, as indicated by the distorted centre-line in Fig. 7.6. Points on the contact surface will undergo tangential displacements $\bar{u}_x$ and $\bar{u}_y$ relative to distant points T_1 and T_2 in the undeformed region of each body. Clearly, if there is no sliding motion between the two bodies as a whole, there must be at least one point at the interface where the surfaces deform without relative motion; but it does not follow

that there is no slip anywhere within the contact area. In fact it will be shown that the effect of a tangential force less than the limiting friction force ($Q < \mu P$) is to cause a small relative motion, referred to as 'slip' or 'micro-slip', over part of the interface. The remainder of the interface deforms without relative motion and in such regions the surfaces are said to adhere or to 'stick'.

To proceed with an analysis we must consider the conditions governing 'stick' and 'slip'. In Fig. 7.6, A_1 and A_2 denote two points on the interface which were coincident before the application of the tangential force. Under the action of the force, points in the body such as T_1 and T_2, distant from the interface, move through effectively rigid displacements δ_{x1}, δ_{y1} and δ_{x2}, δ_{y2} while A_1 and A_2 experience tangential elastic displacements $\bar{u}_{x1}, \bar{u}_{y1}$ and $\bar{u}_{x2}, \bar{u}_{y2}$ relative to T_1 and T_2. If the absolute displacements of A_1 and A_2 (i.e. relative to O) are denoted by s_{x1}, s_{y1} and s_{x2}, s_{y2}, the components of slip between A_1 and A_2 may be written

$$\begin{aligned} s_x \equiv s_{x1} - s_{x2} &= (\bar{u}_{x1} - \delta_{x1}) - (\bar{u}_{x2} - \delta_{x2}) \\ &= (\bar{u}_{x1} - \bar{u}_{x2}) - (\delta_{x1} - \delta_{x2}) \end{aligned} \tag{7.16}$$

A similar relation governs the tangential displacements in the y-direction. If the points A_1 and A_2 are located in a 'stick' region the slip s_x and s_y will be zero so

Fig. 7.6

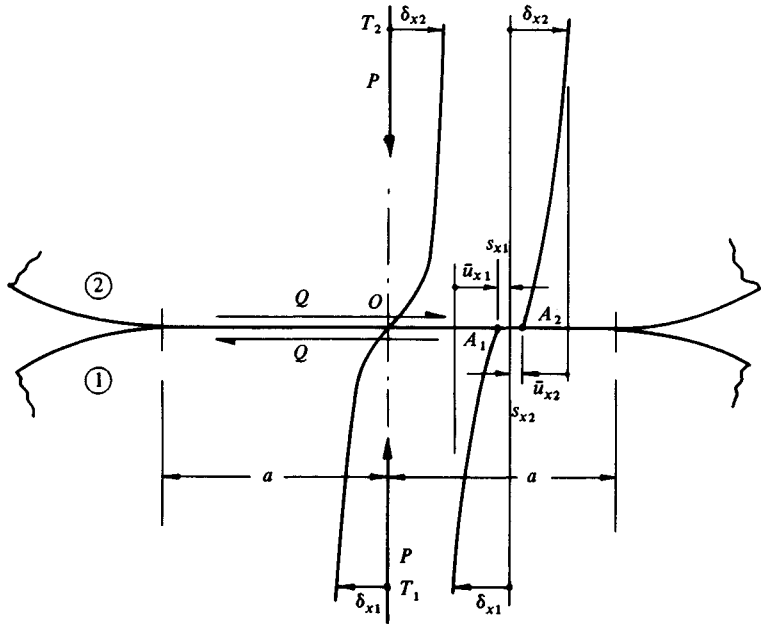

https://doi.org/10.1017/CBO9781139171731.008 Published online by Cambridge University Press

that

$$\bar{u}_{x1} - \bar{u}_{x2} = (\delta_{x1} - \delta_{x2}) \equiv \delta_x \tag{7.17a}$$

$$\bar{u}_{y1} - \bar{u}_{y2} = (\delta_{y1} - \delta_{y2}) \equiv \delta_y \tag{7.17b}$$

We note that the right-hand sides of equations (7.17) denote relative tangential displacements between the two bodies as a whole under the action of the tangential force. Thus δ_x and δ_y are constant, independent of the position of A_1 and A_2, within the 'stick' region. Further, if the two bodies have the same elastic moduli, since they are subjected to mutually equal and opposite surface tractions, we can say at once that $\bar{u}_{x2} = -\bar{u}_{x1}$ and $\bar{u}_{y2} = -\bar{u}_{y1}$. The condition of no slip embodied in equations (7.17) can then be stated: *all surface points within a 'stick' region undergo the same tangential displacement.* The statement is also true when the elastic constants are different but the overall relative displacements δ_x and δ_y are then divided unequally between the two bodies according to equation (7.2).

At points within a stick region the resultant tangential traction cannot exceed its limiting value. Assuming Amonton's law of friction with a constant coefficient μ, this restriction may be stated:

$$|q(x,y)| \leqslant \mu |p(x,y)| \tag{7.18}$$

In a region where the surfaces slip, the conditions of equations (7.17) are violated, but the tangential and normal tractions are related by

$$|q(x,y)| = \mu |p(x,y)| \tag{7.19}$$

In addition, the direction of the frictional traction q must oppose the direction of slip. Thus

$$\frac{q(x,y)}{|q(x,y)|} = -\frac{s(x,y)}{|s(x,y)|} \tag{7.20}$$

Equations (7.17)–(7.20) provide boundary conditions which must be satisfied by the surface tractions and surface displacements at the contact interface. Equations (7.17) and (7.18) apply in a stick region and equations (7.19) and (7.20) apply in a slip region. Difficulty arises in the solution of such problems because the division of the contact area into stick and slip regions is not known in advance and must be found by trial. In these circumstances a useful first step is to assume that no slip occurs anywhere in the contact area. Slip is then likely to occur in those regions where the tangential traction, so found, exceeds its limiting value.

A few particular cases will now be examined in detail.

(a) Two-dimensional contact of cylinders - no slip

We shall first consider two cylinders in contact with their axes parallel to the y-axis, compressed by a normal force P per unit axial length, to which

https://doi.org/10.1017/CBO9781139171731.008 Published online by Cambridge University Press

a tangential force Q per unit length ($<\mu P$) is subsequently applied (see Fig. 7.7). The contact width and the pressure distribution due to P are given by the Hertz theory. These quantities are assumed to be unaffected by the subsequent application of Q. In view of the difficulty of knowing whether Q causes any micro-slip and, if so, where it occurs, we start by assuming that the coefficient of friction is sufficiently high to prevent slip throughout the whole contact area. Thus the complete strip $-a \leqslant x \leqslant a$ is a 'stick' area in which the condition of no-slip (eq. (7.17)) applies, i.e.

$$\bar{u}_{x1} - \bar{u}_{x2} = \text{constant} = \delta_x, \quad -a \leqslant x \leqslant a \tag{7.21}$$

The distribution of tangential traction at the interface is thus one which will give rise to a constant tangential displacement of the contact strip. For the purpose of finding the unknown traction each cylinder is regarded as a half-space to which the results of Chapter 2 apply. The analogous problem of finding the distribution of *pressure* which gives rise to a constant *normal* displacement, i.e.

Fig. 7.7. Contact of cylinders with their axes parallel. Surface tractions and displacements due to a tangential force $Q < \mu P$. Curve A – no slip, eq. (7.22); curve B – partial slip, eq. (7.28).

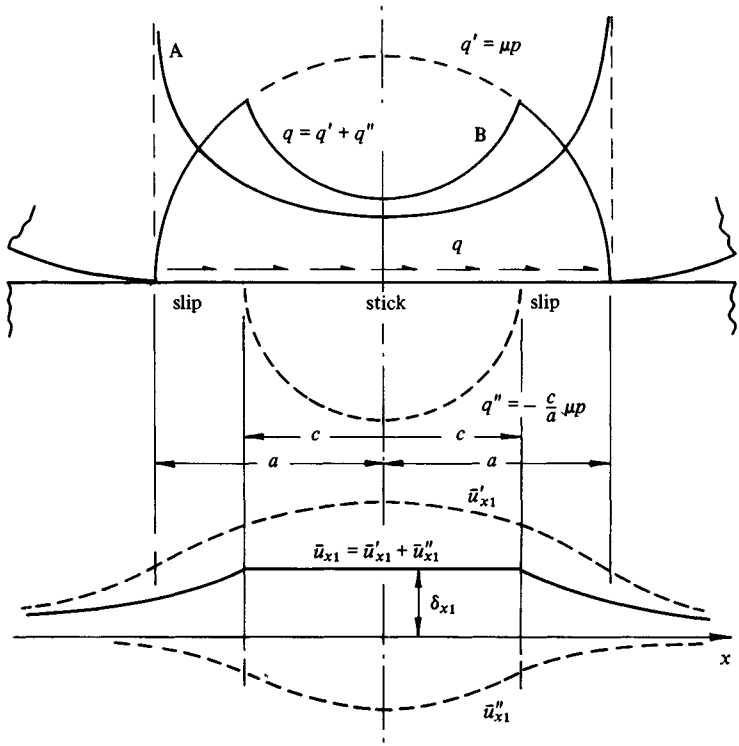

https://doi.org/10.1017/CBO9781139171731.008 Published online by Cambridge University Press

the pressure on the face of a flat frictionless punch, has been discussed in §2.8. The pressure is given by equation (2.64). Using the analogy between tangential and normal loading of an elastic half-space in plane strain we can immediately write down the required distribution of tangential traction, viz.

$$q(x) = \frac{Q}{\pi(a^2 - x^2)^{1/2}} \tag{7.22}$$

This traction acts on the surface of each body in opposing directions so that $\bar{u}_{x1}$ and $\bar{u}_{x2}$ will be of opposite sign and therefore additive in equation (7.21). The actual values of $\bar{u}_{x1}$ and $\bar{u}_{x2}$ and hence the value of δ_x, as in all two-dimensional problems, depend upon the choice of the reference points T_1 and T_2.

The traction given by (7.22) is plotted in Fig. 7.7 (curve A). It rises to a theoretically infinite value at the edges of the contact. This result is not surprising when it is remembered that the original assumption that there should be no slip at the interface effectively requires that the two bodies should behave as one. The points $x = \pm a$ then appear as the tips of two sharp deep cracks in the sides of a large solid block, where singularities in stress would be expected. It is clear that these high tangential tractions at the edge of the contact area cannot be sustained, since they would require an infinite coefficient of friction. There must be some micro-slip, and the result we have just obtained suggests that it occurs at both edges of the contact strip. We might expect a 'stick' region in the centre of the strip where the tangential traction is low and the pressure high. This possibility will now be investigated.

(b) Contact of cylinders - partial slip

The method of solution to the problem of partial slip was first presented by Cattaneo (1938) and independently by Mindlin (1949).

If the tangential force Q is increased to its limiting value μP, so that the bodies are on the point of sliding, the tangential traction is given by equation (7.4), viz.

$$q'(x) = \mu p_0(1 - x^2/a^2)^{1/2} \tag{7.23}$$

where $p_0 = 2P/\pi a$.

The tangential displacements within the contact surface due to the traction can be found. By analogy with the normal displacements produced by a Hertzian distribution of normal pressure, we conclude that the surface displacements are distributed parabolically within the contact strip. If no slip occurs at the mid-point $x = 0$, then we can write

$$\bar{u}'_{x1} = \delta'_{x1} - (1 - \nu_1^2)\mu p_0 x^2/aE_1 \tag{7.24}$$

https://doi.org/10.1017/CBO9781139171731.008 Published online by Cambridge University Press

and a similar expression of opposite sign for the second surface. These distributions of tangential displacement satisfy equation (7.21) at the origin only; elsewhere in the contact region the surfaces must slip.

We now consider an additional distribution of traction given by

$$q''(x) = -\frac{c}{a}\mu p_0(1 - x^2/c^2)^{1/2} \tag{7.25}$$

acting over the strip $-c \leqslant x \leqslant c$ $(c < a)$, as shown in Fig. 7.7. The tangential displacements produced by this traction within the surface $-c \leqslant x \leqslant c$ follow by analogy with equation (7.24), viz.:

$$\bar{u}''_{x1} = -\delta''_{x1} + \frac{c}{a}(1 - \nu_1^2)\mu p_0 x^2/cE_1 \tag{7.26}$$

If we now superpose the two tractions q' and q'', the resultant displacements within the central strip $-c \leqslant x \leqslant c$ are constant, as shown in Fig. 7.7.

$$\bar{u}_{x1} = \bar{u}'_{x1} + \bar{u}''_{x1} = \delta'_{x1} + \delta''_{x1} = \delta_{x1} \tag{7.27a}$$

and for the second surface to which an equal and opposite traction is applied

$$\bar{u}_{x2} = -\delta_{x2} \tag{7.27b}$$

Substitution for $\bar{u}_{x1}$ and $\bar{u}_{x2}$ in equation (7.21) shows that the condition of no-slip is satisfied in the strip $-c \leqslant x \leqslant c$. Furthermore in this region the resultant traction is given by

$$q(x) = q'(x) + q''(x) = \mu p_0\{(a^2 - x^2)^{1/2} - (c^2 - x^2)^{1/2}\}/a \tag{7.28}$$

which is everywhere less than μp. Thus the two necessary conditions that the central strip should be a 'stick' region are satisfied. At the edges of the contact, $c \leqslant |x| \leqslant a$, $q(x) = \mu p(x)$, as required in a slip region. It remains to prove that the direction of the traction opposes the direction of slip in these regions as required by equation (7.20). To do this we require the surface displacements in these regions. The surface displacements due to an elliptical distribution of tangential traction have been evaluated by Poritsky (1950), from which $\bar{u}'_{x1}$ and $\bar{u}''_{x1}$ throughout the surface are plotted (dotted) in Fig. 7.7. From equation (7.16) the slip s_x is given by

$$s_x = (\bar{u}_{x1} - \bar{u}_{x2}) - \delta_x$$

From the figure it is clear that $(\bar{u}_{x1} - \bar{u}_{x2})$ is less than δ_x in each slip region, so that s_x is negative in each region. This is consistent with the positive traction q acting on body (1). We have shown, therefore, that the resultant distribution of tangential traction shown in Fig. 7.7 produces surface displacements which satisfy the necessary conditions in a central stick region $-c \leqslant x \leqslant c$ and two peripheral slip regions $c \leqslant |x| \leqslant a$.

The size of the stick region is determined by the magnitude of the tangential force

$$Q = \int_{-a}^{a} q(x)\,dx = \int_{-a}^{a} q'(x)\,dx + \int_{-c}^{c} q''(x)\,dx$$

$$= \mu P - \frac{c^2}{a^2}\mu P$$

so that

$$\frac{c}{a} = \left(1 - \frac{Q}{\mu P}\right)^{1/2} \tag{7.29}$$

The physical behaviour is now clear. If, keeping P constant, Q is increased steadily from zero, micro-slip begins immediately at the two edges of the contact area and spreads inwards according to equation (7.29). As Q approaches μP, c approaches zero and the stick region shrinks to a line at $x = 0$. Any attempt to increase Q in excess of μP causes the contact to slide.

The stresses within either solid due to the elliptical distribution of traction $q'(x)$ have been discussed in the last section. The stresses due to a force Q less than μP can be found by superposing a distribution of stress due to $q''(x)$ which is similar in form but is reduced in scale.

(c) Contact of spheres - no slip

Two spherical bodies pressed into contact by a normal force P have a circular area of contact whose radius is given by equation (4.22) and an ellipsoidal pressure distribution given by equation (3.39). If a tangential force Q, applied subsequently, causes elastic deformation without slip at the interface, then it follows from equation (7.17) that the tangential displacement of all points in the contact area is the same. If the force Q is taken to act parallel to the x-axis, then it follows from symmetry that this tangential displacement must also be parallel to the x-axis. The distribution of tangential traction which produces a uniform tangential displacement of a circular region on the surface of an elastic half-space has been found in Chapter 3. The traction (equation (3.82)) is radially symmetrical in magnitude and everywhere parallel to the x-axis:

$$q_x(r) = q_0(1 - r^2/a^2)^{-1/2} \tag{7.30}$$

from which $q_0 = Q_x/2\pi a^2$. The corresponding displacement, which, in this case, can be precisely defined, is given by equation (3.86*a*) i.e.

$$\bar{u}_x = \frac{\pi(2-\nu)}{4G}\, q_0 a \tag{7.31}$$

https://doi.org/10.1017/CBO9781139171731.008 Published online by Cambridge University Press

Substituting into equation (7.17) gives the relative tangential displacement between distant points T_1 and T_2 in the two bodies:

$$\delta_x = \bar{u}_{x1} - \bar{u}_{x2} = \frac{Q_x}{8a}\left(\frac{2-\nu_1}{G_1} + \frac{2-\nu_2}{G_2}\right) \tag{7.32}$$

This relationship is shown by the broken line in Fig. 7.8; the tangential displacement is directly proportional to the tangential force. This is unlike the normal approach of two elastic bodies which varies in a nonlinear way with normal load because the contact area grows as the load is increased.

The tangential traction necessary for no slip rises to a theoretically infinite value at the periphery of the contact circle so that some micro-slip is inevitable at the edge of contact.

(d) Contact of spheres - partial slip

Cattaneo's technique can also be applied to the case of spheres in contact. The axial symmetry of the tangential traction given by equation (7.30) suggests that the 'stick' region in this case might be circular and concentric with the contact circle. On the point of sliding, when only the two points in contact at the origin are 'stuck', the distribution of traction is

$$q'(x,y) = \mu p(x,y) = \mu p_0(1 - r^2/a^2)^{1/2} \tag{7.33}$$

The tangential displacements within the contact circle, $r \leqslant a$, are then given by

Fig. 7.8. Tangential displacement δ_x of a circular contact by a tangential force Q_x; (A) with no slip, (B) with slip at the periphery of the contact.

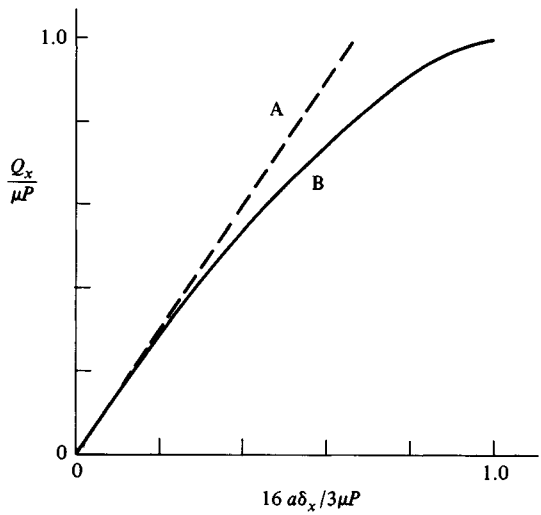

https://doi.org/10.1017/CBO9781139171731.008 Published online by Cambridge University Press

equations (3.91), viz.:

$$\bar{u}'_x = \frac{\pi\mu p_0}{32Ga}\{4(2-\nu)a^2 + (4-\nu)x^2 + (4-3\nu)y^2\} \tag{7.34a}$$

and

$$\bar{u}'_y = \frac{\pi\mu p_0}{32Ga}\, 2\nu xy \tag{7.34b}$$

If we now consider a distribution of traction

$$q''(x,y) = -\frac{c}{a}p_0(1-r^2/c^2)^{1/2} \tag{7.35}$$

acting over the circular area $r \leqslant c$, by analogy the tangential displacements within that circle are

$$\bar{u}''_x = -\frac{c}{a}\frac{\pi\mu p_0}{32Gc}\{4(2-\nu)c^2 + (4-\nu)x^2 + (4-3\nu)y^2\} \tag{7.36a}$$

$$\bar{u}''_y = -\frac{c}{a}\frac{\pi\mu p_0}{32Gc}\, 2\nu xy \tag{7.36b}$$

The resultant displacements in the circle, $r \leqslant c$, are given by adding equations (7.34) and (7.36), with the result:

$$\bar{u}_x = \frac{\pi\mu p_0}{8Ga}(2-\nu)(a^2-c^2) \tag{7.37a}$$

$$\bar{u}_y = 0 \tag{7.37b}$$

We see that these displacements satisfy the condition for no-slip (7.17) within the circle $r \leqslant c$, with the result that

$$\delta_x = \frac{3\mu P}{16}\left(\frac{2-\nu_1}{G_1} + \frac{2-\nu_2}{G_2}\right)\frac{a^2-c^2}{a^3} \tag{7.38}$$

Thus the stick region is the circle of radius c whose value can be found from the magnitude of the tangential force.

$$Q_x = \int_0^a 2\pi q' r\, \mathrm{d}r - \int_0^c 2\pi q'' r\, \mathrm{d}r = \mu P(1 - c^3/a^3)$$

whence

$$\frac{c}{a} = (1 - Q/\mu P)^{1/3} \tag{7.39}$$

The tangential traction acts parallel to the x-axis at all points; it is given by q' (eq. (7.33)) in the annulus $c \leqslant r \leqslant a$ and by the resultant of q' and q'' (which

https://doi.org/10.1017/CBO9781139171731.008 Published online by Cambridge University Press

is less than μp) in the central circle $r \leqslant c$. To confirm that the slip conditions are satisfied in the annulus $c \leqslant r \leqslant a$, the displacements in that annulus due to q'' are required. These are given in equations (3.92). The relative slip at any point in the annulus is then found from equation (7.16) which, in this case, becomes

$$s_x = (\bar{u}'_{x1} + \bar{u}''_{x1}) + (\bar{u}'_{x2} + \bar{u}''_{x2}) - \delta_x \tag{7.40a}$$

and

$$s_y = (\bar{u}'_{y1} + \bar{u}''_{y1}) + (\bar{u}'_{y2} + \bar{u}''_{y2}) \tag{7.40b}$$

where δ_x is given by (7.38), $\bar{u}'_x$ and $\bar{u}'_y$ are given by (7.34), $\bar{u}''_x$ and $\bar{u}''_y$ are given by (3.92). It is clear from the form of equations (3.92*b*) that, when substituted into equation (7.40*b*), the slip in the y-direction will not vanish, i.e. $s_y \neq 0$. On the other hand the frictional traction in the slip annulus, q', is assumed to be everywhere parallel to the x-axis, so that the condition that the slip must be in the direction of the frictional traction is not precisely satisfied. However, we note that the ratio of s_y to s_x is of the order $\nu/(4-2\nu) \approx 0.09$ so that the inclination of the resultant slip direction to the x-axis will not be more than a few degrees. We conclude, therefore, that the distribution of tangential traction which has been postulated, acting everywhere parallel to the tangential force, is a good approximation to the exact solution.

As the tangential force is increased from zero, keeping the normal force constant, the stick region decreases in size according to equation (7.39). An annulus of slip penetrates from the edge of the contact area until, when $Q_x = \mu P$, the stick region has dwindled to a single point at the origin and the bodies are on the point of sliding.

The magnitude of the slip at a radius r within the annulus $c \leqslant r \leqslant a$ is found from equation (7.40). Neglecting terms of order $\nu/(4-2\nu)$ this turns out to be

$$s_x \approx \frac{3\mu P}{16Ga}(2-\nu) \times \left\{\left(1 - \frac{2}{\pi}\sin^{-1}\frac{c}{r}\right)\left(1 - 2\frac{c^2}{r^2}\right) + \frac{2}{\pi}\frac{c}{r}\left(1 - \frac{c^2}{r^2}\right)^{1/2}\right\} \tag{7.41a}$$

$$s_y \approx 0 \tag{7.41b}$$

The maximum value of this micro-slip occurs at the edge of the contact.

The relative tangential displacement of the two bodies is found by substituting equation (7.39) into (7.38)

$$\delta_x = \frac{3\mu P}{16a}\left(\frac{2-\nu_1}{G_1} + \frac{2-\nu_2}{G_2}\right)\left\{1 - \left(1 - \frac{Q_x}{\mu P}\right)^{2/3}\right\} \tag{7.42}$$

https://doi.org/10.1017/CBO9781139171731.008 Published online by Cambridge University Press

This nonlinear expression is also plotted in Fig. 7.8. For very small values of tangential force, when the slip annulus is very thin, it follows the linear relationship for no-slip (eq. (7.32)). As Q approaches μP the tangential displacement departs further from the no-slip solution until the point of sliding is reached. On the point of sliding, the overall displacement δ_x is just twice the relative slip s_x at the edge of the contact circle. Experimental measurements of the displacement by Johnson (1955) substantiate equation (7.42).

It is instructive to compare the compliance of two spherical bodies to tangential force with the compliance to normal force found from the Hertz theory (eq. (4.23)). Since the normal displacement δ_z is nonlinear with load, it is most meaningful to compare the *rates* of change of displacement with load. For bodies having the same elastic constants, differentiating equation (4.23) gives a normal compliance

$$\frac{d\delta_z}{dP} = \tfrac{2}{3}\left\{\tfrac{9}{4}\left(\frac{1-\nu^2}{E}\right)^2\left(\frac{1}{R_1}+\frac{1}{R_2}\right)\frac{1}{P}\right\}^{1/3}$$

$$= \frac{(1-\nu)}{2Ga} \tag{7.43}$$

The tangential compliance for small values of Q_x is given by equation (7.32):

$$\frac{d\delta_x}{dQ_x} = \frac{(2-\nu)}{4Ga} \tag{7.44}$$

So that the ratio of the tangential to normal compliance is $(2-\nu)/2(1-\nu)$, which varies from 1.17 to 1.5 as Poisson's ratio varies from 0.25 to 0.5 and is independent of the normal load. Thus the tangential and normal compliances are roughly similar in magnitude.

Non-conforming surfaces of general profile will have an elliptical contact area under normal load. Their behaviour under the action of a subsequently applied tangential force is qualitatively the same as for spherical bodies. Microslip occurs at the edge of the contact area and a stick area is found which is elliptical in shape and which has the same eccentricity as the contact ellipse. Expressions for the tangential displacement have been found by Mindlin (1949) for the case of no-slip and by Deresiewicz (1957) for partial slip.

7.3 Simultaneous variation of normal and tangential forces

In the previous section we discussed the contact stresses introduced by a steadily increasing tangential force into two bodies which were pressed into contact by a normal force which was maintained constant. We saw that the tangential force, however small, causes some slip to occur over part of the contact area. The 'irreversibility' implied by frictional slip suggests that the

final state of contact stress will depend upon the history of loading and not solely upon the final values of the normal and tangential forces. Two examples demonstrate that this is indeed the case.

In the problem of the last section, in which the normal force was kept constant and the tangential force was increased, the annulus of slip spread inwards from its inner boundary. If, on the other hand, the tangential force were subsequently *decreased* this process would not simply reverse. Instead micro-slip *in the opposite direction* would begin at the edge of the contact. Hence the state of stress during unloading is different from that during loading, showing that the process is irreversible. We shall return to this problem in the next section.

As a second example, consider the case where tangential force, having been applied, is kept constant while the normal force is varied. Increasing the normal force increases the area of contact, but leaves the tangential traction unchanged, so that a traction-free annulus grows at the edge of the contact area. Decreasing the normal force causes a reduction in the contact area and thereby releases some of the tangential traction. In order to maintain equilibrium with the constant tangential force the inner boundary of the annulus of slip must contract until eventually, when P reaches the value Q/μ, the contact will slide. Clearly, in this example also, the behaviour in normal unloading is different from that during loading.

It is evident from the foregoing discussion that the state of contact stress between two bodies subjected to variations in normal and tangential load is dependent upon the sequence of application of the loads, so that the surface tractions can only be determined with certainty by following, in incremental steps, the complete loading history. In a paper of considerable complexity Mindlin & Deresiewicz (1953) have investigated the changes in surface traction and compliance between spherical bodies in contact arising from the various possible combinations of incremental change in loads: P increasing, Q increasing; P decreasing, Q increasing; P increasing, Q decreasing; etc. In this way it is possible to build up the stress and displacement variation throughout any prescribed sequence of loading.

In this section we shall consider just one example of practical interest. Two spherical bodies, pressed together initially by a normal force P_0, are subsequently compressed by an increasing oblique force F, which is inclined at a constant angle α to the common normal. This loading is equivalent to increasing the tangential load Q and the normal load P by increments in the constant proportion $\tan\alpha$ (see Fig. 7.9).

The contact radius is determined by the current value of the total normal load according to the Hertz theory (eq. (4.22)) which may be written

$$a^3 = KP \tag{7.45}$$

https://doi.org/10.1017/CBO9781139171731.008 Published online by Cambridge University Press

Due to the initial normal load

$$a_0^3 = KP_0 \tag{7.46}$$

During the subsequent application of the oblique force F, the increments in tangential and normal force are $\mathrm{d}Q = \mathrm{d}F \sin \alpha$ and $\mathrm{d}P = \mathrm{d}F \cos \alpha$ respectively. The incremental growth of the contact radius is given by differentiating (7.45), thus

$$3a^2 \,\mathrm{d}a = K \,\mathrm{d}P = K \,\mathrm{d}Q/\tan \alpha \tag{7.47}$$

We will assume first that the increment of tangential force does not give rise to any slip. The consequent increment in tangential traction is then given by equation (7.30), viz.:

$$\mathrm{d}q(r) = \frac{\mathrm{d}Q}{2\pi a}(a^2 - r^2)^{-1/2} \tag{7.48}$$

To find the resultant distribution of tangential traction when the contact radius has grown to the value a, we substitute for $\mathrm{d}Q$ in (7.48) from (7.47) and integrate with respect to a.

For points originally within the contact circle the lower limit of integration is a_0, but points lying outside the original contact only start to acquire tangential traction when the contact circle has grown to include them, so that the lower limit of integration is then r.

Fig. 7.9. Circular contact subjected to a steady normal load P_0 and an oblique force F. A – $\tan \alpha < \mu$ (no micro-slip); B – $\tan \alpha > \mu$ (slip in annulus $c \leqslant r \leqslant a$).

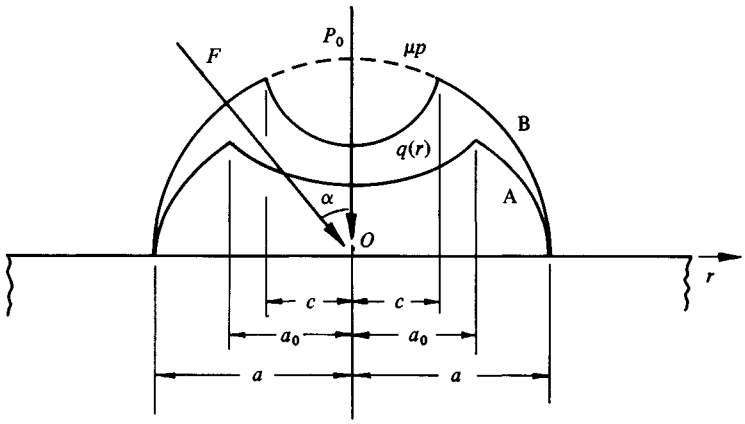

https://doi.org/10.1017/CBO9781139171731.008 Published online by Cambridge University Press

$$q(r) = \frac{3\tan\alpha}{2\pi K}\int_{a_0}^{a_1} a(a^2 - r^2)^{-1/2}\,\mathrm{d}a$$

$$= \frac{3\tan\alpha}{2\pi K}\{(a_1^2 - r^2)^{1/2} - (a_0^2 - r^2)^{1/2}\}, \quad 0 \leqslant r \leqslant a_0 \qquad (7.49a)$$

and

$$q(r) = \frac{3\tan\alpha}{2\pi K}\int_{r}^{a_1} a(a^2 - r^2)^{-1/2}\,\mathrm{d}a$$

$$= \frac{3\tan\alpha}{2\pi K}(a_1^2 - r^2)^{1/2}, \quad a_0 \leqslant r \leqslant a_1 \qquad (7.49b)$$

The normal pressure at this stage of loading is given by the Hertz theory:

$$p(r) = \frac{3(P_0 + F_1\cos\alpha)}{2\pi a_1^3}(a_1^2 - r^2)^{1/2}$$

$$= \frac{3}{2\pi K}(a_1^2 - r^2)^{1/2} \qquad (7.50)$$

For our original assumption of no slip to be valid, $q(r)$ must not exceed $\mu p(r)$ at any point. This condition is satisfied provided that

$$\tan\alpha \leqslant \mu \qquad (7.51)$$

Thus an oblique force inclined to the normal axis at an angle less than the angle of friction produces no micro-slip within the contact area. The consequent distribution of traction is shown in Fig. 7.9, curve A; it is everywhere less than the limiting value $\mu p(r)$.

On the other hand, if the inclination of the force F exceeds the angle of friction, some slip must occur and the above analysis breaks down. An annulus of slip must develop at the edge of the contact circle. Within this annulus the tangential traction will maintain its limiting value $\mu p(r)$ at all stages of the oblique loading. The inner boundary of the annulus will lie within the original contact circle, its value being determined by the usual condition of equilibrium with the tangential force, whence

$$1 - \frac{c^3}{a^3} = \frac{F\sin\alpha}{\mu(P_0 + F\cos\alpha)} \qquad (7.52)$$

This state of affairs is shown in Fig. 7.9, curve B. The stick region will vanish ($c = 0$) and sliding will begin when

$$F = \frac{\mu P_0}{\cos\alpha\,(\tan\alpha - \mu)} \qquad (7.53)$$

https://doi.org/10.1017/CBO9781139171731.008 Published online by Cambridge University Press

In the case where there is no initial compression the above results reduce to the elementary rule of dry friction: if the inclination of the oblique force is less than the angle of friction no slip will occur and, moreover, the distribution of frictional stress at the interface is everywhere proportional to the normal contact pressure, ($q = p \tan \alpha$); if the inclination of the force exceeds the angle of friction, sliding begins at once and the frictional traction is everywhere equal to its limiting value ($q = \mu p$).

7.4 Oscillating forces

In this section we examine contacts which are compressed by a steady mean normal load P_0 while being subjected to an oscillating force of prescribed amplitude. It will be taken for granted that the magnitude of the oscillating force is insufficient to cause the two surfaces in contact to separate or to slide at any instant during the loading cycle.

We shall consider first an oscillating *tangential* force of amplitude $\pm Q_*$ applied to spherical surfaces in contact. Since the normal force remains constant at P_0, the contact area and the normal pressure will remain constant and as given by Hertz. The first application of Q in a positive direction will cause micro-slip in the annulus $c \leqslant r \leqslant a$, where

$$c/a = (1 - Q/\mu P_0)^{1/3}$$

in the manner discussed in §2. The distribution of tangential traction is shown by curve A in Fig. 7.10(a); it reaches its limiting value in the positive sense in the annulus of slip. The tangential displacement of one body relative to the other is given by equation (7.42), and shown by OA in Fig. 7.10(b). At point A on this curve $Q = +Q_*$. The tangential force now begins to decrease, which is equivalent to the application of a *negative* increment in Q. If there were no slip during this reduction, the increment in tangential traction would be negative and infinite at the edge of the contact area. Hence there must be some negative slip immediately unloading starts and the tangential traction near to the edge must take the value $q(r) = -\mu p(r)$. During the unloading the reversed slip penetrates to a radius c' and, within this radius, there is no reversed slip. The increment in tangential traction due to unloading, by Cattaneo's technique, is therefore

$$\Delta q = -2\frac{3\mu P_0}{2\pi a^3}(a^2 - r^2)^{1/2}, \quad c' \leqslant r \leqslant a \tag{7.54a}$$

and

$$\Delta q = -2\frac{3\mu P_0}{2\pi a^3}\{(a^2 - r^2)^{1/2} - (c'^2 - r^2)^{1/2}\}, \quad r \leqslant c' \tag{7.54b}$$

https://doi.org/10.1017/CBO9781139171731.008 Published online by Cambridge University Press

Fig. 7.10. Circular contact subjected to a steady normal load P_0 and an oscillating tangential load of amplitude Q_*. (*a*) Traction distributions at A ($Q = Q_*$); B ($Q = 0$) and C ($Q = -Q_*$). (*b*) Load–displacement cycle.

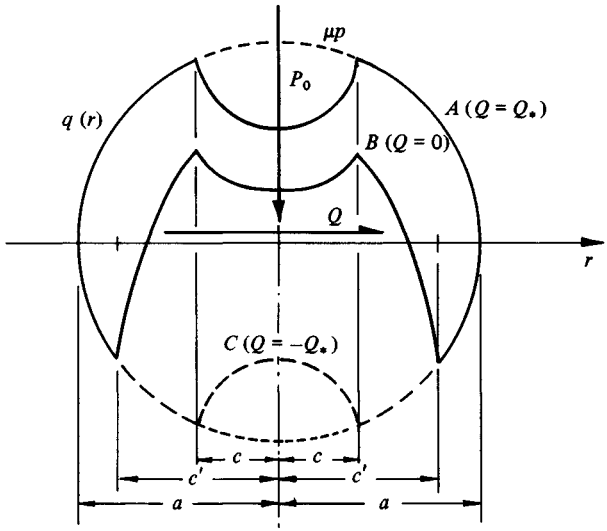

(*a*)

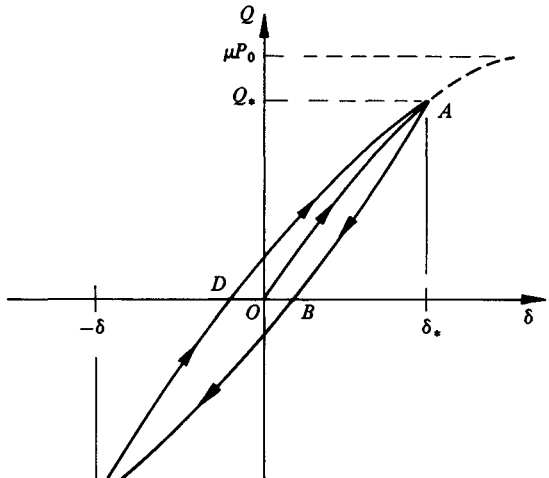

(*b*)

https://doi.org/10.1017/CBO9781139171731.008 Published online by Cambridge University Press

The resultant traction at a point on the unloading curve is then given by adding this increment to the traction at A with the result:

$$q = \begin{cases} -\dfrac{3\mu P_0}{2\pi a^3}(a^2 - r^2)^{1/2}, & c' \leqslant r \leqslant a \qquad (7.55a) \\ -\dfrac{3\mu P_0}{2\pi a^3}\{(a^2 - r^2)^{1/2} - 2(c'^2 - r^2)^{1/2}\}, & c \leqslant r \leqslant c' \qquad (7.55b) \\ -\dfrac{3\mu P_0}{2\pi a^3}\{(a^2 - r^2)^{1/2} - 2(c'^2 - r^2)^{1/2} + (c^2 - r^2)^{1/2}\}, & r \leqslant c \qquad (7.55c) \end{cases}$$

as shown by curve B in Fig. 7.10(a). The radii of the stick regions are found from equilibrium of the traction distribution given above with the applied force. At point A

$$\frac{Q_*}{\mu P_0} = 1 - c_*^3/a^3 \qquad (7.56)$$

During unloading

$$\frac{Q}{\mu P_0} = \frac{Q_*}{\mu P_0} - \frac{\Delta Q}{\mu P_0} = (1 - c_*^3/a^3) - 2(1 - c'^3/a^3) \qquad (7.57)$$

which fixes the extent of reversed slip c'/a. At point B, when the tangential load is removed, $Q = 0$, so that

$$c'^3/a^3 = \tfrac{1}{2}(1 + c_*^3/a^3) \qquad (7.58)$$

The tangential displacement during unloading is found using equation (7.38), viz.:

$$\begin{aligned} \delta &= \delta_* - \Delta\delta \\ &= \frac{3\mu P_0}{16a^3}\left(\frac{2-\nu_1}{G_1} + \frac{2-\nu_2}{G_2}\right)\{(a^2 - c_*^2) - 2(a^2 - c'^2)\} \\ &= \frac{3\mu P_0}{16a}\left(\frac{2-\nu_1}{G_1} + \frac{2-\nu_2}{G_2}\right)\left\{2\left(1 - \frac{Q_* - Q}{2\mu P_0}\right)^{2/3} \right. \\ &\quad \left. - \left(1 - \frac{Q_*}{\mu P_0}\right)^{2/3} - 1\right\} \end{aligned} \qquad (7.59)$$

This expression is shown in Fig. 7.10(b) by the curve ABC. At point C, when the tangential force is completely reversed, substituting $Q = -Q_*$ in equations (7.57) and (7.59) gives

$$c = c_* \quad \text{and} \quad \delta = -\delta_*$$

Thus the reversed slip has covered the original slip annulus and the distribution of tangential traction is equal to that at A, but of opposite sign. The conditions at C are a complete reversal of those at A, so that a further reversal of Q produces

https://doi.org/10.1017/CBO9781139171731.008 Published online by Cambridge University Press

a sequence of events which is similar to unloading from A, but of opposite sign. The displacement curve CDA completes a symmetrical hysteresis loop.

The work done by the tangential force during a complete cycle, represented by the area of the loop, is dissipated by a reversal of micro-slip in the annulus $c \leqslant r \leqslant a$. This problem was first studied by Mindlin *et al.* (1952), who derived an expression for the energy dissipated per cycle, viz.:

$$\Delta W = \frac{9\mu^2 P_0^2}{10a}\left(\frac{2-\nu_1}{G_1}+\frac{2-\nu_2}{G_2}\right) \times \left[1-\left(1-\frac{Q_*}{\mu P_0}\right)^{5/3}-\frac{5Q_*}{6\mu P_0}\left\{1-\left(1-\frac{Q_*}{\mu P_0}\right)^{2/3}\right\}\right] \tag{7.60}$$

During repeated oscillation a tangential force might be expected to produce some attrition of interface in the annulus where oscillating slip is taking place. Measurements by Goodman & Brown (1962) of the energy dissipated in micro-slip compare favourably with equation (7.60).

We turn now to the case where the line of action of the oscillating force $\pm F_*$ is not tangential to the surface, but makes a constant angle α to the z-axis. If the inclination of the force is less than the angle of friction, we saw in the last section that the first application of the oblique force F causes no slip anywhere in the contact area. The derivation of this result is equally applicable when F is decreasing, so no slip would be expected and hence no energy would be dissipated in a cycle of oscillation.

When the inclination of the force exceeds the angle of friction, slip arises on first loading and on unloading. Mindlin & Deresiewicz (1953) have traced the variations in slip, traction and tangential compliance when two spherical bodies, compressed by a steady normal load P_0, are subjected to a cyclic oblique force F which oscillates between the extreme values F_* and $-F_*$. They show that the first loading from $F = 0$ to $F = +F_*$ and the first unloading from $F = +F_*$ to $F = -F_*$ are unique. Subsequently a steady cycle is repeated. The contact radius varies from a_* to a_{-*} determined by the maximum and minimum values of the normal load, i.e. $P_0 \pm F_* \cos\alpha$. Oscillating slip occurs in the annulus $c_* \leqslant r \leqslant a_*$, where

$$\left(\frac{c_*}{a_*}\right)^3 = \frac{P_0 - F_*(\sin\alpha)/\mu}{P_0 + F_* \cos\alpha} \tag{7.61}$$

The energy dissipated per cycle in oscillating slip is shown to be:

$$\Delta W = \frac{9(\mu P_0)^2}{10a_0}\left(\frac{2-\nu_1}{G_1}+\frac{2-\nu_2}{G_2}\right)\left[\frac{1}{4\lambda}\left\{\frac{1+\lambda}{1-\lambda}(1-\lambda L_*)^{5/3} - \frac{1-\lambda}{1+\lambda}(1+\lambda L_*)^{5/3}\right\} - \frac{6-L_*-5\lambda^2 L_*}{6(1-\lambda^2)}(1-L_*)^{2/3}\right] \tag{7.62}$$

https://doi.org/10.1017/CBO9781139171731.008 Published online by Cambridge University Press

where $L_* = F_* \sin \alpha/\mu P_0$, $\lambda = \mu/\tan \alpha$ and a_0 is the contact radius due to P_0. If the force acts in a tangential direction, $\alpha = \pi/2$ and $\lambda = 0$. Equation (7.62) then reduces to equation (7.60). When the angle α diminishes to the value $\tan^{-1} \mu$, $\lambda = 1$ and the energy loss given by (7.62) vanishes.

This interesting result - that oscillating forces, however small their amplitude compared with the steady compressive load, produce oscillating slip and consequent energy dissipation if their inclination to the normal exceeds the angle of friction - has been subjected to experimental scrutiny by Johnson (1961) using a hard steel sphere in contact with a hard flat surface. The angle of friction was approximately 29° ($\mu \approx 0.56$). Photographs of the surface attrition due to repeated cycles of oscillating force are shown in Fig. 7.11. Measurements of the energy dissipated per cycle at various amplitudes of force F_* and angles of obliquity α are plotted in Fig. 7.12. Serious surface damage is seen to begin

Fig. 7.11. Annuli of slip and fretting at the contact of a steel sphere and flat produced by an oscillating oblique force at an angle α to the normal.

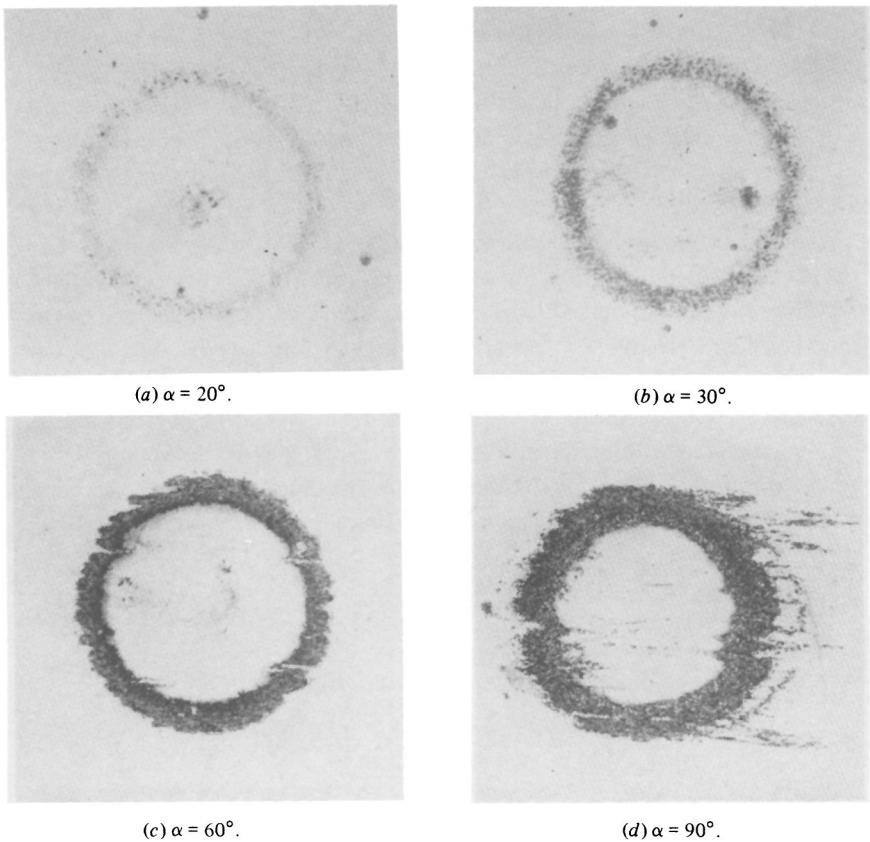

(*a*) $\alpha = 20°$. (*b*) $\alpha = 30°$.

(*c*) $\alpha = 60°$. (*d*) $\alpha = 90°$.

https://doi.org/10.1017/CBO9781139171731.008 Published online by Cambridge University Press

at values of α in excess of 29°, when the theory would predict the onset of slip, and the severity of attrition is much increased as α approaches 90°. This is consistent with the large increase in energy dissipated as the angle α is increased. There is generally reasonable agreement between the measured energy dissipation and that predicted by equation (7.62), taking $\mu = 0.56$. The small energy loss measured at $\alpha = 0$ is due to elastic hysteresis.

It is evident from Fig. 7.11 that some slight surface damage occurred at angles at which no slip would be expected. More severe damage has been observed by Tyler *et al.* (1963), within the annulus $a_* < r < a_{-*}$, under the action of a purely normal load. The difference in curvature between the sphere and the mating flat surface must lead to tangential friction and possible slip, but this effect is very much of second order and cannot be analysed using small-strain elastic theory. It is more likely that the damage is associated with plastic deformation of the surface asperities.

The contact problems involving oscillating forces discussed in this section are relevant to various situations of engineering interest. Oscillating micro-slip at

Fig. 7.12. Energy dissipated in micro-slip when a circular contact is subjected to a steady load P_0 and an oscillating oblique force of amplitude F_* at an angle α to the normal. Eq. (7.62) compared with experimental results (Johnson, 1961).

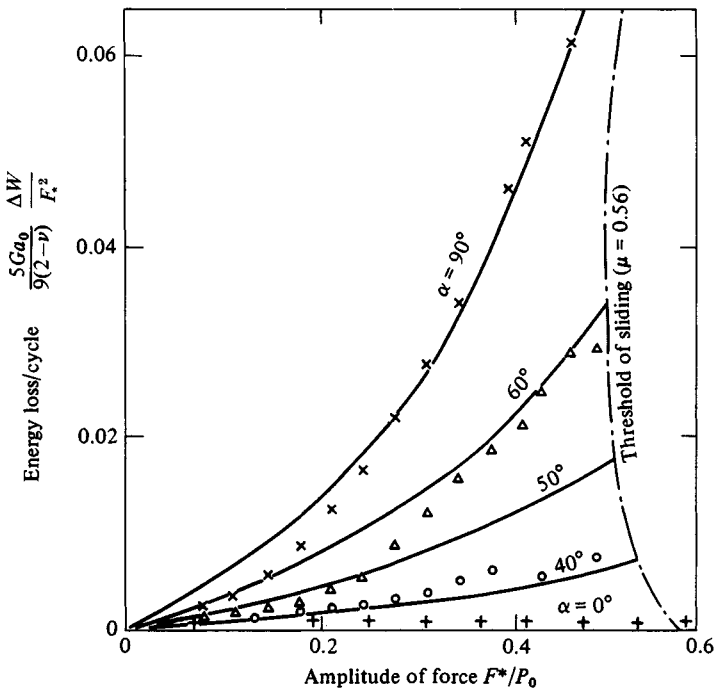

https://doi.org/10.1017/CBO9781139171731.008 Published online by Cambridge University Press

the interface between two surfaces which are subjected to vibration, often combined with corrosion, produces the characteristic surface damage described as 'fretting'. In components which also carry a high steady stress, the presence of fretting can lead to premature failure of the component by fatigue. An ideal solution to this problem is to eliminate the possibility of micro-slip. From the examples discussed in this section, two lessons can be learnt. Firstly, the design should be arranged so that the line of action of the oscillating force is close to the direction of the common normal to the two mating surfaces. Secondly, the profiles of the two contacting surfaces should be designed so that, when they are in contact and under load, high concentrations of tangential traction at the edge of the contact area are avoided. This means that the 'sharp notch' which arises at the edge of the contact of non-conforming surfaces must be avoided. Such a modification to prevent micro-slip is illustrated in Fig. 7.13. These questions have been discussed in a paper by Johnson & O'Connor (1964).

The energy dissipated in micro-slip at surfaces in contact provides one source of vibration damping in a built-up mechanical structure. In particular we have seen how slip and frictional damping may be expected even though the amplitude of the oscillating force transmitted by the surfaces in contact is only a small fraction of the force necessary to cause bulk sliding at the interface. If the amplitude of oscillation is small, i.e. if $Q_*/\mu P_0 \ll 1.0$, equation (7.60) for the energy loss per cycle reduces to

$$\Delta W = \frac{1}{36a\mu P_0}\left(\frac{2-\nu_1}{G_1}+\frac{2-\nu_2}{G_2}\right) Q_*^{\,3} \tag{7.63}$$

i.e. the energy loss is proportional to the *cube* of the amplitude of the oscillating force. The same is true for an oblique force (eq. (7.62)). In a review of the damping in built-up structures arising from interfacial slip Goodman (1960) shows that the variation of energy loss with the cube of the amplitude is a general rule which applies to clamped joints having a variety of geometric forms. These cases all have one feature in common: they develop a region of micro-slip which

Fig. 7.13. Influence of the profiles of contacting bodies on micro-slip and fretting.

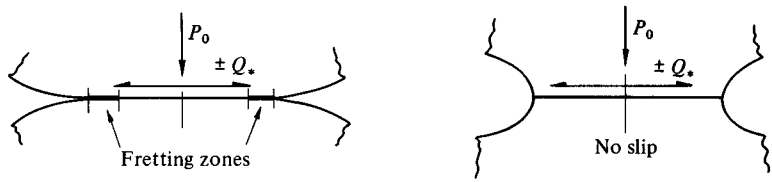

(*a*) (*b*)

https://doi.org/10.1017/CBO9781139171731.008 Published online by Cambridge University Press

grows in size in direct proportion to amplitude of the force. Experimental measurements of slip damping however tend to result in energy losses which are more nearly proportional to the *square* of the amplitude at small amplitudes. In part this discrepancy between theory and experiments is due to inelastic effects within the body of the solids (internal hysteresis damping) which provide a large proportion of the measured damping at small amplitudes. But variations in the coefficient of friction and effects of roughness of the experimental surface are also influential (see Johnson, 1961).

A third practical application of the contact stress theory discussed in this section lies in the mechanics of granular media. Mindlin and his colleagues used the compliance of elastic spheres in contact to calculate the speed of propagation of elastic waves through an idealised granular 'solid' made up of elastic spheres packed in a regular array. This work is summarised by Mindlin (1954) and by Deresiewicz (1958).

7.5 Torsion of elastic spheres in contact

A situation which is qualitatively similar to those discussed in the previous sections of this chapter arises when two elastic solids are pressed together by a constant normal force and are then subjected to a varying twisting or 'spinning' moment about the axis of their common normal. The physical behaviour is easy to visualise. The normal force produces an area of contact and distribution of normal pressure given by the Hertz theory. The twisting moment causes one body to rotate about the z-axis through a small angle β relative to the other. Slip at the interface is resisted by frictional traction. Each body is regarded as an elastic half-space from the point of view of calculating its elastic deformation. Under the action of a purely twisting couple M_z the state of stress in each body is purely torsional, i.e. all the direct stress components vanish, as discussed in §3.9. In the case of spheres in contact the system is axi-symmetrical; $\tau_{r\theta}$ and $\tau_{z\theta}$ are the only non-zero stress components and u_θ is the only non-zero displacement.

If there were to be no slip at the interface, it follows that the contact surface must undergo a rigid rotation relative to distant points in each body. Thus

$$\bar{u}_{\theta 1} = \beta_1 r, \quad \bar{u}_{\theta 2} = -\beta_2 r$$

The distribution of tangential traction to produce a rigid rotation of a circular region on the surface of an elastic half-space is shown to be (equations (3.109) and (3.111))

$$q(r) = \frac{3M_z r}{4\pi a^3}(a^2 - r^2)^{-1/2} \tag{7.64}$$

where $q(r)$ acts in a circumferential direction at all points in the contact circle

https://doi.org/10.1017/CBO9781139171731.008 Published online by Cambridge University Press

$r \leqslant a$. The rotation is given by

$$\beta = \beta_1 + \beta_2 = \tfrac{3}{16}\left(\frac{1}{G_1} + \frac{1}{G_2}\right)\frac{M_z}{a^3} \tag{7.65}$$

A similar result for bodies of general profile, whose area of contact is elliptical, follows from equations (3.114) and (3.115).

As we might expect, the surface traction to prevent slip entirely, given by equation (7.64), rises to infinity at the edge of the contact circle so that an annular region of slip will develop. This slip will be in a circumferential direction and the surface traction in the slip annulus $c \leqslant r \leqslant a$ will take its limiting value

$$q(r) = \mu p(r) = \frac{3\mu P}{2\pi a^3}(a^2 - r^2)^{1/2} \tag{7.66}$$

Fig. 7.14. A circular contact area subjected to a twisting moment M_z. (*a*) Shear traction $q(r/a)$: A – no slip, eq. (7.64); B – partial slip, taking $c = a/\sqrt{2}$. (*b*) Angle of twist β: A – no slip; B with slip.

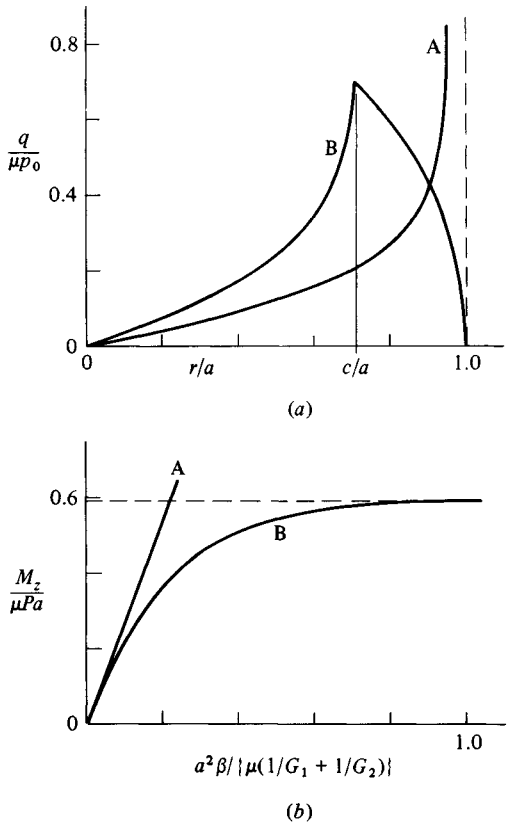

https://doi.org/10.1017/CBO9781139171731.008 Published online by Cambridge University Press

The radius c of the stick region is given by

$$\frac{3}{4\pi}(1-c^2/a^2)\left(\frac{1}{G_1}+\frac{1}{G_2}\right)\mathbf{D}(k)=a^2\beta/\mu P \tag{7.67}$$

where $\mathbf{D}(k)=\mathbf{K}(k)-\mathbf{E}(k)$; $k=(1-c^2/a^2)^{1/2}$, and $\mathbf{K}(k)$ and $\mathbf{E}(k)$ are complete elliptic integrals of the first and second kind respectively. The distribution of traction in the stick circle and the relation between the twisting moment M_z and the angle of twist β are shown in Fig. 7.14(*a*) and 7.14(*b*) respectively. These results are due to Lubkin (1951).

As the twisting moment is increased the radius of the stick region decreases and eventually shrinks to a point in the centre. One body is then free to 'spin' relative to the other resisted by a constant moment

$$M_z=3\pi\mu Pa/16 \tag{7.68}$$

The shear stress reaches its limiting value at all points. The state of stress within the solid under the combined action of this tangential traction and the Hertz pressure has been investigated by Hetenyi & McDonald (see §3.9).

Spherical bodies in contact which are subjected to an oscillating twisting moment $\pm M_z^*$ have been studied by Deresiewicz (1954). Unloading after the application of a moment M_z^* leads to a reversal of micro-slip at the edge of the contact circle with consequent hysteresis in the angle of twist. In a complete oscillation of the moment a hysteresis loop is traced out, similar to the loop arising from an oscillating tangential force shown in Fig. 7.10. Deresiewicz shows that the energy dissipated per cycle, represented by the area of the hysteresis loop, is given by

$$\Delta W=\frac{2\mu^2P^2}{Ga}\left[\tfrac{8}{9}\left\{1-\left(1-\tfrac{3}{2}\frac{M_z^*}{\mu Pa}\right)^{2/3}\right\}-\frac{M_z^*}{\mu Pa}\left\{1+\left(1-\tfrac{3}{2}\frac{M_z^*}{\mu Pa}\right)^{1/2}\right\}\right] \tag{7.69}$$

For small amplitudes ($M_z^* \ll \mu Pa$) this expression reduces to

$$\Delta W\approx 3M_z^{*3}/16Ga^4\mu P \tag{7.70}$$

in which the energy loss per cycle is again proportional to the cube of the amplitude of the twisting moment.

7.6 Sliding of rigid-perfectly-plastic bodies

In §6.2 we considered the contact of perfectly plastic bodies under the action of normal compression. The plastic deformation was regarded as sufficiently large to justify neglecting the elastic strains and applying the theory of rigid-perfectly-plastic solids. We shall now consider such contacts to which

https://doi.org/10.1017/CBO9781139171731.008 Published online by Cambridge University Press

tangential as well as normal forces are applied so that sliding motion or, at least, incipient sliding occurs. The analyses presented in this section have been applied mainly to the interaction between the irregularities on the sliding surfaces of ductile solids and thereby relate to theories of friction and wear (see Bowden & Tabor, 1951). The simplest example which has been solved completely is that of a plastic wedge which is compressed and subsequently sheared (Johnson, 1968*a*). We shall take this example first.

(a) Combined shear and pressure on a plastic wedge

A rigid-perfectly-plastic wedge, of semi-angle α, is deformed by a rigid flat die. If the interface were frictionless no tangential force could be realised, so that sliding could not contribute to the deformation. We shall assume the opposite extreme: that there is no slip at the interface.

Under an initial compressive load P the wedge is crushed as described in §6.2(*c*) and shown in Fig. 6.8(*b*). The pressure on the die face is given by equation (6.28) viz.:

$$p_0 = P/l_0 = 2k(1 + \psi_0)$$

The normal force is now kept constant and a steadily increasing tangential force Q is applied, which introduces a shear traction q at the interface and causes the slip lines to meet the die face at angles $\pi/4 \pm \phi$. The slip-line field for the combined action of P and Q is shown in Fig. 7.15(*a*). The triangle ABC adheres to the face of the die and moves with it both normally and tangentially. Triangles BDE and EHJ also move as rigid blocks. The left-hand shoulder of the wedge (apex A) is unloaded by Q and does not deform further. At the stage of the process shown in Fig. 7.15(*a*) the die pressure is

$$p = k(1 + 2\psi + \cos 2\phi) = p_0 - 2k(\phi - \sin^2 \phi) \tag{7.71}$$

and the shear stress on the die face is

$$q = 2k \sin \phi \cos \phi \tag{7.72}$$

Hence

$$\frac{Q}{P} = \frac{q}{p} = \frac{\sin \phi \cos \phi}{(1 + \psi_0) - (\phi + \sin^2 \phi)} \tag{7.73}$$

As the tangential force is increased, ϕ increases and, in due course, $\phi = \pi/4$. A second stage of deformation is then reached, illustrated in Fig. 7.15(*b*), in which

$$p = k(1 + 2\psi) \tag{7.74}$$

and

$$q = k = \text{constant} \tag{7.75}$$

https://doi.org/10.1017/CBO9781139171731.008 Published online by Cambridge University Press

hence

$$\frac{Q}{P} = \frac{1}{1 + 2\psi} \tag{7.76}$$

Further increases in Q causes the block BHJ to rotate clockwise so that ψ steadily decreases to zero and Q/P approaches unity. At this point sliding might be expected by shear of the interface AB. With real materials, which strain-harden, it seems likely that further bulk deformation could occur by shearing virgin material along a slip line from A to J.

It is apparent from the analysis that the tangential force Q causes an increase in contact area even though the normal load P remains constant. This process has been called 'junction growth' by Tabor (1959). In plane deformation the

Fig. 7.15. Combined shear and pressure on a rigid-perfectly-plastic wedge ($\alpha = 60°$): (*a*) first stage ($Q/P < 0.72$); (*b*) second stage ($0.72 < Q/P < 1.0$).

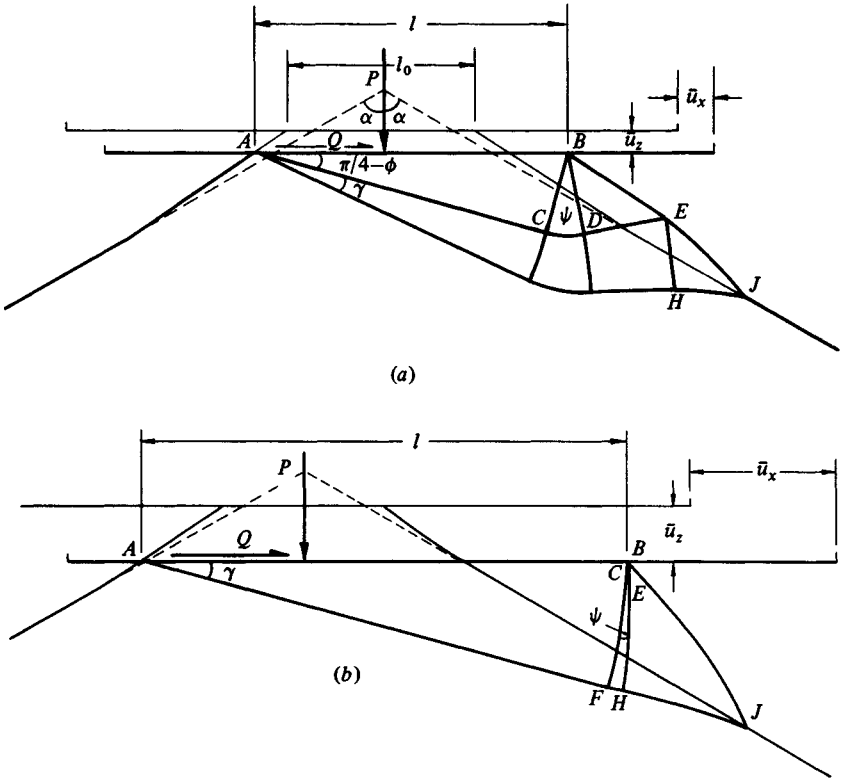

https://doi.org/10.1017/CBO9781139171731.008 Published online by Cambridge University Press

area increase is given by

$$\frac{A}{A_0} = \frac{l}{l_0} = \frac{p_0}{p} \tag{7.77}$$

where p is given by equations (7.71) and (7.74). The area growth for a wedge of angle $\alpha = 60°$ is shown in Fig. 7.16.

So far it has been assumed that adhesion between the wedge and the die is sufficient to prevent sliding at the interface. The shear stress at the interface is also plotted against Q/P in Fig. 7.16. If, due to contamination or lubrication, the shear strength of the interface is less than that of the solid k, then the process of plastic deformation and area growth will be interrupted by premature sliding at the interface. Fig. 7.16 is instructive in relation to metallic friction: it shows the importance of surface contamination upon the effective coefficient of limiting friction. For example, if the maximum shear stress which the interface can sustain is reduced by contamination to one half the shear strength of the metal (Q/P) is only 0.15. At the other extreme, if the strength of the interface approaches k, the analysis suggests that the coefficient of friction approaches 1.0, a value which is consistent with experiments on a chemically clean ductile material.

Collins (1980) has examined the situation where a wedge is deformed by a rigid flat die under the action of normal and tangential forces which increase

Fig. 7.16. Contact area growth of plastic wedge ($\alpha = 60°$) under the action of a constant normal load P and an increasing tangential load Q.

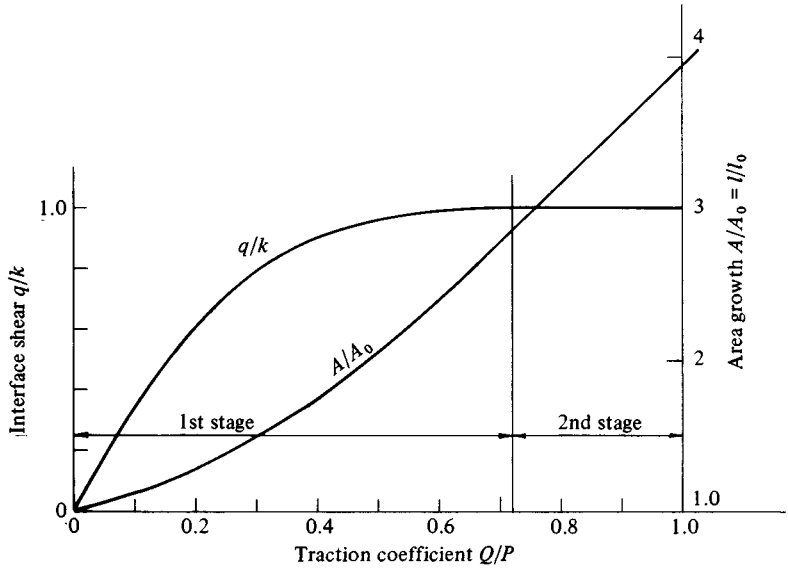

https://doi.org/10.1017/CBO9781139171731.008 Published online by Cambridge University Press

in a fixed ratio. At small or moderate ratios of Q/P the modes of deformation of the wedge are similar to those shown in Fig. 7.15. For a ratio $Q/P \to 1.0$ a different mode of deformation is possible in which a spiral chip is formed as shown in Fig. 7.17(*b*). Experiments suggest that this mode of deformation may also occur in the case of a constant normal load discussed previously, when $Q/P \to 1.0$, if the material is capable of strain hardening.

Fig. 7.17. Application of an oblique force to a plastic wedge. When $Q/P \to 1.0$ a 'curly chip' is formed (Collins, 1980).

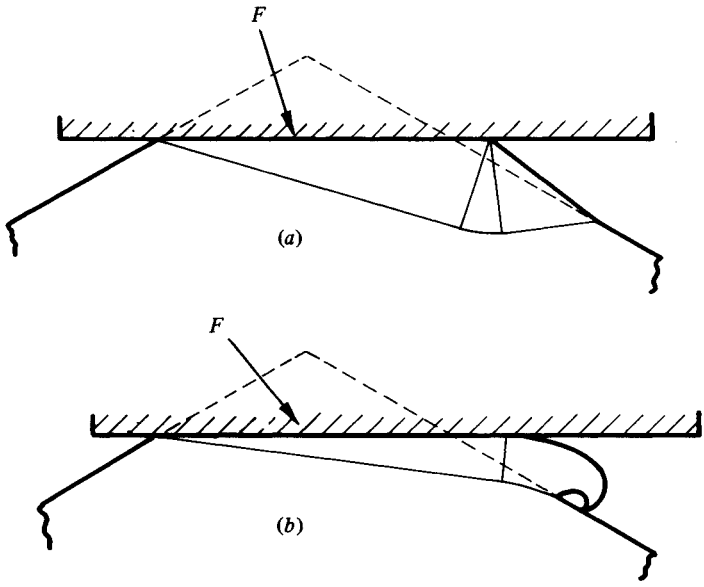

(b) Ploughing of a rigid-plastic surface by a rigid wedge

In this example we consider a rigid-perfectly-plastic half-space which is indented by a rigid wedge and is subsequently ploughed by the action of a tangential force applied to the wedge perpendicular to its axis. In the first instance we shall take the faces of the wedge to be frictionless. The deformation is determined by constructing slip-line fields and their associated hodographs progressively in the stages shown in Fig. 7.18. In stage (1) the application of the normal load P alone produces an indentation of depth c_0 as shown. The subsequent application of a steadily increasing tangential force Q, whilst keeping P constant, unloads the left-hand face of the wedge so that further deformation takes place by the wedge sliding down the left-hand shoulder of the initial indentation. The wedge continues to slide deeper until $Q = P \tan \alpha$, when the

https://doi.org/10.1017/CBO9781139171731.008 Published online by Cambridge University Press

pressure on the left-hand face of the wedge has fallen to zero (stage 2). During subsequent deformation the force F on the active face of the wedge remains constant ($=P$ cosec α). As material from the trough is displaced into the prow, the wedge rides up on its own 'bow wave' such that the contact length h satisfies the relationship:

$$F = ph = 2k(1 + \psi)h = \text{constant} \tag{7.78}$$

As deformation proceeds (stages 3–6) the apex of the wedge approaches the free surface asymptotically. In the steady state a plastic wave is pushed along the surface, like a wrinkle in a carpet, giving a permanent shear displacement δ to the surface layer of the half-space. The steady-state behaviour ($\alpha < \pi/4$) is illustrated in Fig. 7.19(*a*). In this condition

$$\left.\begin{aligned} p_s &= 2k(1 + \psi_s) = 2k(1 - \pi/2 + 2\alpha) \\ P &= p_s h_s \sin\alpha; \quad Q = p_s h_s \cos\alpha \end{aligned}\right\} \tag{7.79}$$

Through the progressive construction of the slip-line fields and hodographs the trajectory followed by the apex of the wedge can be found and is plotted in Fig. 7.20. In common with crushing a plastic wedge, the application of tangential force causes the surfaces firstly to sink together, thereby increasing the area of contact and decreasing the contact pressure. In the case of the indenting wedge, this first stage is followed by a period in which the wedge climbs back to the surface pushing a plastic 'wave' ahead of it along the surface.

Friction at the wedge face modifies the behaviour described above. Moderate friction causes the slip lines to meet the wedge face at $\pi/4 \pm \phi$, but severe friction results in adhesion between the wedge face and the solid. Initial penetration then follows the field shown in Fig. 6.5 or 6.6. As a tangential force is applied the wedge sinks in further, at 45° to begin with, and then at the angle of the wedge face. Proceeding as before progressive construction of the slip-line fields and hodographs enables the trajectory of the wedge and forces on the wedge face

Fig. 7.18. Ploughing of a rigid-plastic surface by a rigid frictionless wedge ($\alpha = 60°$), under the action of a steady normal load P and an increasing tangential force Q. Progressive stages of deformation.

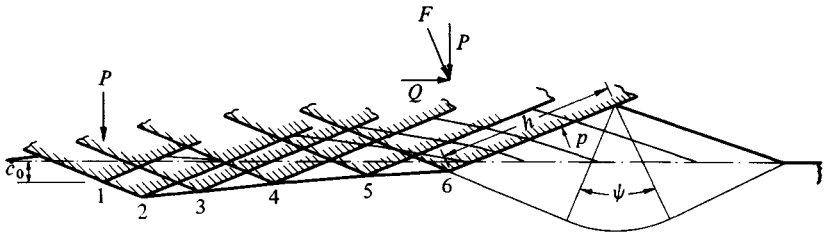

https://doi.org/10.1017/CBO9781139171731.008 Published online by Cambridge University Press

Fig. 7.19. Plastic bow wave produced by the steady-state sliding of a rigid wedge over a perfectly plastic surface: (*a*) frictionless; (*b*) with no slip at the wedge face.

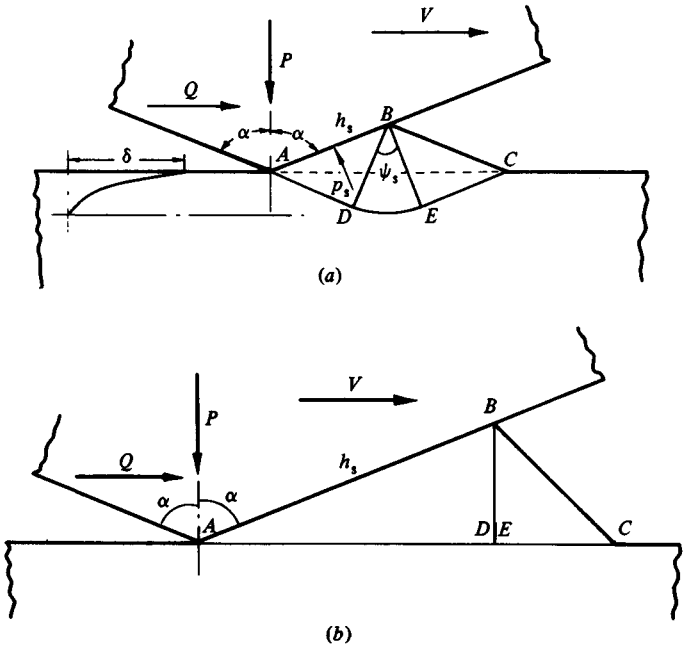

Fig. 7.20. Transient ploughing of a plastic surface by a rigid wedge: ratio of tangential to normal force Q/P; ratio of shear stress to normal pressure q/p on wedge face; depth of penetration δ/c_0.

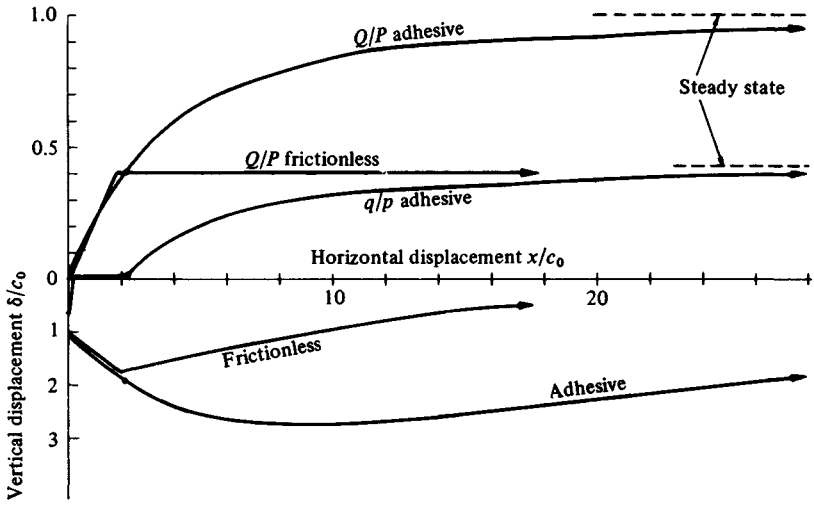

https://doi.org/10.1017/CBO9781139171731.008 Published online by Cambridge University Press

to be found (see Fig. 7.20). The adhesive wedge ploughs much deeper than the frictionless wedge and builds up a larger prow ahead. The situation in the limit when the wedge reaches the surface level is shown in Fig. 7.19(*b*). At this stage the ratio Q/P approaches unity and the prow is free to shear off along the slip line *ADEC*. The ratio q/p of shear to normal traction on the wedge face during the process is also plotted in Fig. 7.20. For adhesion to be maintained throughout, the coefficient of friction between the wedge face and the solid must exceed $\cot \alpha$.

The development of a prow of heavily deformed material in the manner just described has been demonstrated by Cocks (1962) and others in sliding experiments with clean ductile metals. Challen & Oxley (1979) refer to a plastic wave (Fig. 7.19(*a*)) as the 'rubbing mode' of deformation, since material is smeared along the surface without being detached. They refer to the deformation shown in Fig. 7.19(*b*), in which a prow builds up and may become detached, as the 'wear mode' and investigate the conditions of wedge angle and interfacial friction which lead to one mode or the other. They also show that a third mode – the 'cutting mode' – is possible; the wedge does not rise to the level of the free surface but produces a continuous chip in the manner of a cutting tool.

(c) Interaction of two rigid-plastic wedges

In the study of sliding friction between rough metal surfaces, the interaction of two wedges, which interfere and mutually deform as they pass, is of interest. The situation is different from the above examples in that the relative motion of the two wedges is taken to be purely tangential. In these circumstances both the tangential force Q and the normal force P vary throughout a contact cycle; indeed, with strong adhesion at the interface, P becomes *tensile* just before the wedges separate.

Slip-line fields for the initial deformation have been proposed by Green (1954). Complete cycles of contact have been analysed by Edwards & Halling (1968*a* & *b*), using the approximate 'upper bound' method, which are in reasonable agreement with experiments (see also Greenwood and Tabor, 1955).

(d) Ploughing by three-dimensional indenters

Most practical instances of ploughing, the action of a grit on a grinding wheel for example, involve three-dimensional deformation; a furrow is produced and material is displaced sideways. The simplest model of this process is that of a rigid cone or pyramid sliding steadily over the surface, but even these cases are difficult to analyse.

By assuming a simple mode of deformation in which a cap of material adheres to the front of the cone, Childs (1970) has used the plastic work method to obtain approximate values for the tangential force Q to plough a furrow of prescribed depth. Material from the furrow is ploughed into shoulders on either side. Good agreement was found with measurements of the ploughing force, but the height of the shoulders was observed to be appreciably less than in the theoretical deformation mode.